3rd European supercritical CO2 Conference
September 19-20, 2019, Paris, France

2019-sCO2.eu-138

MODELLING AND OPTIMISATION OF SUPERCRITICAL CARBON DIOXIDE TURBOMACHINERY

Ruan van der Westhuizen*
Stellenbosch University
Stellenbosch, South Africa
Email: rvanderwesthuizen@sun.ac.za

Johan van der Spuy
Stellenbosch University
Stellenbosch, South Africa

Albert Groenwold
Stellenbosch University
Stellenbosch, South Africa

Robert Dobson
Stellenbosch University
Stellenbosch, South Africa

ABSTRACT

In this work models of a centrifugal compressor and radial inflow turbine are presented. The models serve as a way to perform the initial design of the turbomachines for application in small- to medium-scale power cycles. The models are based on the classical mean-line velocity triangle approach which is supplemented with loss coefficients. Restrictive assumptions are not placed on the fluid and therefore the models can be used with supercritical carbon dioxide as will be explored in this work. In order to gain insight into the relationship between the geometrical specifications, thermodynamic operating conditions and performance characteristics of the turbomachinery, mathematical optimisation is performed for specific objectives under given constraints. The benefit of this is that the inevitable trade-offs between the design variables can be studied a priori, before any physical prototypes are built. Results are presented as Pareto plots between pairs of design variables. The importance of choosing an appropriate objective function and upper and lower bounds on the variables is discussed as well.

INTRODUCTION AND BACKGROUND

As a working fluid for power cycles, supercritical carbon dioxide (sCO_2) has many benefits. Above turbine inlet temperatures of 550°C, it can be shown that an sCO_2 Brayton cycle can achieve a higher thermodynamic efficiency than cycles that use other working fluids [1]. Furthermore, the performance of small sCO_2 Brayton cycles with simple layouts is comparable to much larger and more complicated steam Rankine cycle systems [1].

The performance of a Brayton power cycle is dominated by the performance of the turbomachinery [2]. Many variables have an influence on the performance of a turbomachine and it is a challenging engineering problem to find values for these variables that will lead to a well-designed machine.

New turbomachines have predominantly been designed by iterating on previous designs [3]. This is achieved through the use of basic theoretical principles and correlations that have been developed from empirical testing. Whilst this approach has proven to be technically successful and commercially viable for steam and gas turbomachinery, the sCO_2 turbomachinery industry is still relatively undeveloped. As a result, empirical correlations for sCO_2 turbomachinery are unavailable.

Another problem with this approach is that it is based on trial-and-error methods that are informed almost entirely by the knowledge and experience of the turbomachinery designer. Global optimisation is therefore not possible. Computational fluid dynamics (CFD) is a suitable alternative turbomachinery design tool and is amenable to more rigorous optimisation [4]; but the drawback of this approach is that CFD simulations are computationally expensive and unsuitable for system-level design and optimisation work.

The accuracy of CFD-derived performance analysis can be combined with the speed of gradient-based optimisation through the use of a *response surface model* (RSM) in which the effect of the design variables on the objective function of the optimisation are approximated [5]. Only a few CFD simulations are performed and the results of the objective function are then correlated to the design variables through a statistical regression analysis that yields a function or a neural network that yields an output value. The RSM then replaces the CFD in the optimisation process. RSM methods have been applied successfully to the optimisation of turbomachinery, including multi-objective (Pareto) optimisation [5, 6].

Despite the advantages of RSM methods, the accuracy of the results depends on the accuracy of the RSM approximation. Given the many variables involved in the analysis of turbomachinery, several CFD simulations are therefore still required in order to develop an accurate RSM.

* corresponding author

DOI: 10.17185/duepublico/48895

The lack of suitable sCO_2 turbomachinery models that are both computationally inexpensive (i.e. do not require substantial CFD simulation work) and amenable to rigorous optimisation has resulted in the design of the turbomachinery receiving little to no attention during the initial design of sCO_2 power cycles. The machines are often modelled simply with a constant efficiency and with scant regard to their physical geometry. Although this may be satisfactory for elementary steady-state design work, it is obviously unsatisfactory for any detailed design work which requires matching of the cycle mass flow rate, proposed temperatures and pressures, and geometrical specifications with each other.

OBJECTIVES

The two common methods of designing and optimising turbomachinery (i.e. by iterating on previous designs or by using CFD simulations) have some drawbacks. This work presents an alternative approach which relies on mathematical models developed from standard theory. These models are required to meet three main objectives which are formalised as follows.

Firstly, the models should be developed as part of a larger power system model. Therefore, the interfaces (i.e. inlet and outlet) between the turbine or compressor stage and the rest of the system should be well-defined – both from a thermodynamic perspective and a geometrical perspective. The models must describe the design and performance of the turbomachines not only in isolation but also when integrated in a system.

Secondly, the models should be developed with robust mathematical gradient-based optimisation in mind as the primary application. This requires that the models consist entirely of a series of mathematical equations that capture the relationships between the variables of the machine.

Finally, given the lack of empirical data on sCO_2 turbomachines, it is conceivable that the current state-of-the-art of sCO_2 turbomachine modelling will be enhanced in the future by more accurate theory, procedures and correlations. In order to accommodate this, the models must be flexible and amenable to updates as required. Notwithstanding this, some applications may desire a faster computation time rather than the utmost modelling accuracy. As a result, the models must be based on the most elementary theoretical principles only. Any additional model complexity should augment rather than replace the basic principles.

MODELLING

The theoretical analysis of turbomachinery has been well-documented. Turbomachinery can be modelled reasonably accurately using only a few basic equations that can be found in most textbooks on turbomachinery (the interpretations of Aungier [3], Dixon and Hall [7], Korpela [8] and Japikse and Baines [9] are good examples). However, authors differ on the specifics of their notation and on the detail of their analyses. Furthermore, any model of a turbomachine must also take into consideration how that model is to be implemented because it will dictate the characteristics that the model should possess.

It is for these reasons that there are no universal analytical models for turbomachinery and it is worthwhile to present an introduction to the analytical turbomachinery models which are implemented in this work.

Consider a *stage* of a generic turbomachine, depicted schematically in Figure 1.

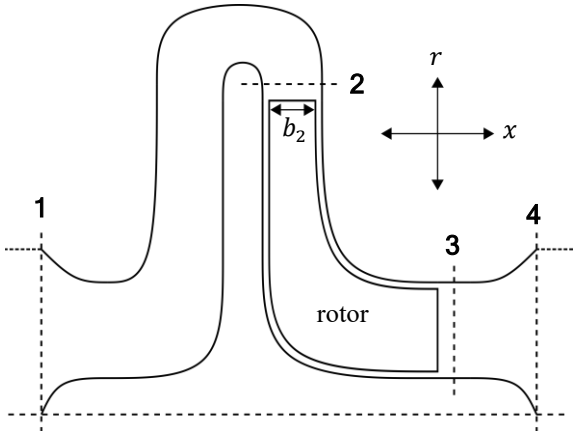

Figure 1: flow stations of a generic turbomachine stage

The stage consists of four main stations where the characteristics of the flow is analysed at. In a turbine, the flow is in the direction 1-2-3-4 and in a compressor the flow direction is reversed: 4-3-2-1. Sections 1-2 and 3-4 are stationary. In a turbine, 1-2 acts as a nozzle which accelerates the flow and 3-4 acts as a diffuser to slow the flow. In a compressor 4-3 is insignificant (and can be ignored) but 2-1 acts as a diffuser.

The *rotor* section between stations 2 and 3 is rotating and the transfer of momentum between the fluid and the blades occurs here.

A front view of the rotor section is depicted in Figure 2. Only one half of the blades are shown. The relevant blade dimensions are indicated. The outer radius of the disk r_2 is referred to as the *tip radius*. At station 3, the inner-most (smallest) radius r_{3h} is the *hub radius* whereas the larger radius r_{3s} corresponds to the *shroud radius*. The direction of rotation of the disk is also indicated in Figure 2: in the ω_T direction for a turbine and in the ω_C direction for a compressor.

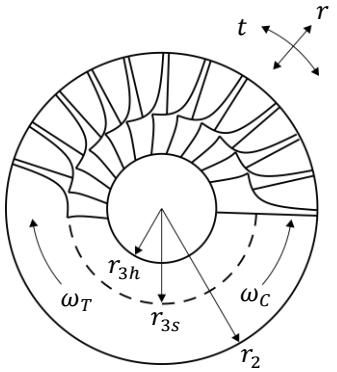

Figure 2: front view of a rotor disk

DOI: 10.17185/duepublico/48895

The geometry of a centrifugal compressor is very similar to the geometry of a radial inflow turbine and therefore common notation can be used. Assuming that the thickness of the blades is negligible, the radial flow area at station 2

$$A_{2r} = 2\pi r_2 b_2 \quad (1)$$

is the circumference of the disk multiplied by the blade width b_2. At station 3 the axial flow area

$$A_{3x} = \pi(r_{3s}^2 - r_{3h}^2) \quad (2)$$

is the annulus between the shroud radius and the hub radius.

The mass flow rate

$$\dot{m} = \rho V_m A \quad (3)$$

is the product of the local density ρ, local absolute velocity V_m in the meridional (m) direction and area A normal to the flow. At station 2, the radial (r) direction is the meridional direction and at stations 1, 3 and 4 the axial (x) direction is the meridional direction. The flow can have a component in the tangential (t) direction at stations 2 and 3, but at stations 1 and 4 it is assumed that the flow has no tangential component. The conservation of mass is enforced as long as the mass flow rate is equal at all four flow stations.

A way to visualise the flow at stations 2 and 3 is to use a *velocity triangle*. A velocity triangle represents the relationship between the absolute velocity V, relative velocity R and blade velocity B.

The sign convention is as follows: the tangential direction is positive in the direction of blade rotation, and the meridional direction is positive in the direction of fluid flow. The angle that the absolute velocity vector makes with the meridional direction is denoted by α and the angle that the relative velocity vector makes with the meridional direction is denoted by β. With the positive meridional direction as reference, if the angle measurement is towards the positive tangential direction, then the angle is considered as positive. Conversely, if the angle measurement is towards the negative tangential direction, then the angle is considered as negative.

Figure 3 depicts a generic velocity triangle that can be used to analyse the flow at stations 2 and 3.

The flow direction is reversed in a compressor as compared to a turbine and the blades rotate in the opposite direction. However, the sign convention remains as previously defined and therefore the same velocity triangle can be used for both a turbine and a compressor.

A velocity triangle can be analysed using simple trigonometric rules that can be found from inspection.

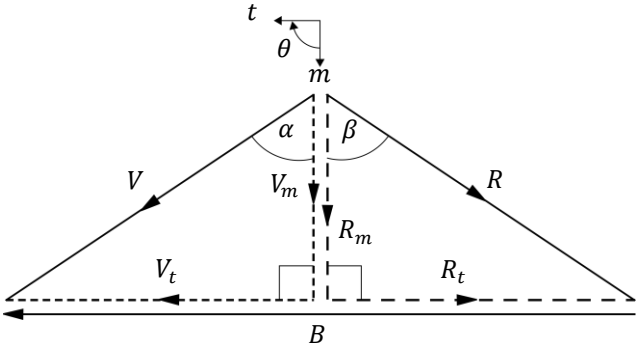

Figure 3: a generic velocity triangle

The relative velocity vector is defined as the vector subtraction of the blade velocity from the absolute velocity. Since the blade velocity only has a component in the tangential direction, this implies that

$$R_t = V_t - B \quad (4)$$

The blade speed

$$B = r\omega \quad (5)$$

can be calculated by multiplying the local radius by the angular velocity ω. At station 2, the tip radius r_2 is used and at station 3 the mean radius r_3 between the hub and shroud is used, where

$$r_3 = \frac{r_{3h} + r_{3s}}{2} \quad . \quad (6)$$

The conservation of momentum is taken into account by considering the resulting moment on the shaft

$$M = \dot{m}(V_{2t} r_2 - V_{3t} r_3) \quad . \quad (7)$$

The fluid power

$$\dot{W}_F = M\omega \quad (8)$$

can be determined by multiplying the moment by the angular velocity at which the shaft is rotating. However, this power is not equivalent to the power obtained from the conservation of energy (the first law of thermodynamics). Ignoring gravitational potential energy, the power obtained by applying the principle of the conservation of energy is

$$\dot{W} = \dot{m}\left[\left(h_2 + \tfrac{1}{2}V_2^2\right) - \left(h_3 + \tfrac{1}{2}V_3^2\right)\right] \quad . \quad (9)$$

The fluid power does not take into account the additional parasitic work terms such as leakage and windage, but the thermodynamic energy equation does [9]. The parasitic work

$$\dot{W}_P = \left|\dot{W} - \dot{W}_F\right| \quad (10)$$

is therefore the difference between the thermodynamic power and the fluid power.

The flow direction is defined in opposite directions for the compressor and turbine cases. This has the consequence that station 2 is always at a higher total enthalpy than station 3 and therefore the power rating is always a positive quantity regardless of whether a turbine or a compressor is under analysis.

The accurate modelling of sCO_2 thermodynamic properties is crucial for developing accurate sCO_2 turbomachinery models. A thermodynamic model of sCO_2 that is accurate across broad ranges of temperature and pressure cannot be based on simplifying assumptions such as the ideal gas or incompressible fluid assumptions.

Apart from evaluating lengthy and computationally expensive equations-of-state, the most accurate thermodynamic model can be achieved by interpolating from finely resolved tables of sCO_2 thermodynamic properties. Unfortunately, such an approach is also computationally expensive because a special interpolating function needs to be called with every iteration. An alternative approach is to use simple correlations of the form

$$x_3 = ax_1 + bx_2 + cx_1^2 + dx_1x_2 + ex_2^2 \ldots \quad (11)$$

where the coefficients $a, b, c, d, e, \ldots$ are determined using a statistical regression analysis of the tabulated data.

This is valid because any thermodynamic property can be calculated if any two other properties are known [10]. It is therefore possible to state that a property x_3 can be expressed as a function of only two other properties x_1 and x_2.

DOI: 10.17185/duepublico/48895

Equation 11 is an example of a second-order correlation, but the correlations can contain an arbitrary number of terms of any order. The more terms the correlations contain, in theory the more closely the properties will resemble the true properties of sCO_2 but the longer each calculation using the correlations will take. If fewer terms are used, then the properties that are calculated from the correlations will begin to deviate from the true properties of sCO_2 but the calculation speed will increase.

Another aspect to consider in the development of the turbomachinery models is the entropy generation or *losses* that occur throughout the stage. This is a fundamental part of accurately predicting turbomachine performance, but it is also the most challenging aspect to model.

There are numerous types of losses that occur throughout a turbomachine stage and there is no universal naming scheme nor is there a universally applicable loss model; in fact there are over 1.5 million possible loss model configurations [11]. Given the complexity of the physics encapsulated by the loss models, they are invariably based on empirically determined coefficients. However, as a result of the lack of empirical sCO_2 turbomachinery data, there are no loss coefficients that are specifically applicable to sCO_2 turbomachinery.

In the current models, three loss coefficients are employed. The first is the *rotor loss coefficient*

$$\zeta_R = \frac{h_0 - h_{0s}}{\frac{1}{2}R_2^2} \tag{12}$$

which represents the difference between actual total enthalpy achieved at the outlet of the rotor section and the total enthalpy that would have been achieved if the process was isentropic, as a fraction of the relative kinetic energy at the tip. The rotor loss coefficient applies to enthalpy values at station 2 in the case of a compressor and at station 3 in the case of a turbine.

The second loss coefficient is the *parasitic work coefficient*

$$\zeta_P = \frac{w_P}{\frac{1}{2}R_2^2} = \frac{\dot{W}_P}{\frac{1}{2}\dot{m}R_2^2} \tag{13}$$

which represents the parasitic work as a fraction of the relative kinetic energy at the tip of the rotor.

In the stationary sections of the turbomachinery (i.e. sections 1-2 and 3-4), the total enthalpy remains constant as a result of no shaft work and an assumption of negligible heat transfer. Only one additional loss factor – the *diffuser efficiency* – is necessary to characterise these sections. To derive the diffuser efficiency, consider the *pressure recovery coefficient* [9] of a diffuser

$$C_p = \frac{P_{\text{out}} - P_{\text{in}}}{P_{0,\text{in}} - P_{\text{in}}} \tag{14}$$

which represents the fraction of the kinetic available at the inlet to the diffuser that is converted into a static pressure rise. The ideal pressure recovery coefficient

$$C_{p,\text{ideal}} = 1 - (AR)^2 \tag{15}$$

is only a function of the area ratio AR. The ratio of the actual pressure recovery coefficient to the ideal pressure recovery coefficient is then defined as the *diffuser efficiency*

$$\eta_D = C_p / C_{p,\text{ideal}} \quad . \tag{16}$$

If the area ratio is defined as

$$AR = \frac{A_{\text{small}}}{A_{\text{large}}} \tag{17}$$

where A_{large} is the larger and A_{small} the smaller of the two flow areas of the section then the diffuser efficiency can be applied to a nozzle as well – the only difference is that the nozzle efficiency will exceed unity because the static pressure is reduced rather than raised [9].

The final factor to consider is *slip* which accounts for the fact that the flow at the tip is not perfectly guided by the blades of a compressor or by the inlet vanes of a turbine. Slip is incorporated into the models of this work by solving a third velocity triangle for each machine: in other words, a velocity triangle at station 3, a no-slip velocity triangle at station 2 and a velocity triangle at station 2 that includes slip. The two velocity triangles at station 2 can be linked through the *slip factor*

$$\sigma = \frac{V_{2t}}{V_{2t}^{'}} \tag{18}$$

where V_{2t} represents the tangential velocity component with slip included and $V_{2t}^{'}$ represents the tangential velocity component without slip.

Although the turbomachinery models developed in this work are similar to the models developed by Da Lio et al. [12] and by Alshammari et al. [13], the computational implementation of the models is significantly different. Before the computational implementation is discussed however, it is necessary to define the concept of a mathematical optimisation problem.

MATHEMATICAL OPTIMISATION

A general constrained mathematical optimisation problem is formulated as [14]

$$\begin{aligned} &\text{minimise } f(\boldsymbol{x}) \text{ subject to} \\ &g_i(\boldsymbol{x}) \leq 0, i = 1,2,\dots,m \\ &h_j(\boldsymbol{x}) = 0, j = 1,2,\dots,r \\ &\text{with } \boldsymbol{x} = [x_1, x_2, \dots, x_n]^{\mathrm{T}} \quad . \end{aligned} \tag{19}$$

The column vector $\boldsymbol{x}$ contains the *design variables* of the problem. The problem has n design variables. These design variables represent the *design* of the system. A particular design can be compared with another design through the *objective function* $f(\boldsymbol{x})$.

The objective function is a function of one or more of the design variables and it has a scalar-valued solution. The objective function represents some kind of performance metric of the system and it is assumed that a smaller value of the objective function represents better performance. The best or *optimal* system design is therefore found when the objective function is minimised. If instead a performance metric should be maximised, then the objective function can simply be negated. All mathematical optimisation problems can therefore be treated as minimisation problems.

DOI: 10.17185/duepublico/48895

Not all system designs are valid designs. In order to restrict the design variables to yield a valid design, the problem is constrained by m inequality constraints $g(\boldsymbol{x})$ and r equality constraints $h(\boldsymbol{x})$. Each constraint is a function of one or more of the design variables.

COMPUTATIONAL IMPLEMENTATION

The scientific computing package MATLAB (version R2018b) by MathWorks includes an optimisation toolbox which has a built-in constrained optimisation algorithm called *fmincon* [15]. The user is required to specify the objective function $f(\boldsymbol{x})$ and a separate function which returns the vectors $\boldsymbol{g}(\boldsymbol{x})$ and $\boldsymbol{h}(\boldsymbol{x})$. which are the solutions to the constraints of the problem at some design $\boldsymbol{x}$.

The equality constraints of the turbomachinery optimisation problem are the model equations developed in this work.

The inequality constraints are used for incorporating factors such as checking that the flow is not choked, that the nozzle section has a converging area ratio and the diffuser sections a diverging area ratio, and that the design variables are within acceptable limits. In particular, the design limits for angles, velocity ratios and geometry ratios as reported by Korpela [8] are used in this work.

The constraints must be written such that all the terms are on the same side of the equation. A valid turbomachinery design (and solution) is therefore found if $\boldsymbol{g}(\boldsymbol{x}) \leq \boldsymbol{0}$ and $\boldsymbol{h}(\boldsymbol{x}) = \boldsymbol{0}$. For practical purposes however, a solution is considered valid as long as

$$\max\big(\boldsymbol{g}(\boldsymbol{x})\big) \leq t_c \approx 0 \tag{20}$$

and

$$\max(|\boldsymbol{h}(\boldsymbol{x})|) \leq t_c \approx 0 \tag{21}$$

where t_c is the *constraint tolerance* (0.001 in this work).

Given a starting point $\boldsymbol{x_0}$, *fmincon* uses a gradient-based optimisation algorithm to attempt to minimise $f(\boldsymbol{x})$ whilst also satisfying Equations 20 and 21. It is the case that for most starting points the optimisation algorithm converges to an invalid solution or the solution converges to a local minimum rather than to the global minimum. It is therefore necessary to solve the problem a large number of times with different starting points throughout the design space. The *design space* is the set of all values of the design variables between their *lower bounds* $\check{\boldsymbol{x}}$ and *upper bounds* $\hat{\boldsymbol{x}}$. All variables are given finite bounds.

MODEL CALIBRATION AND VERIFICATION

The loss coefficients introduced in Equations 12, 13 and 16 and the slip factor introduced in Equation 18 require numerical values before the turbomachinery models can be completed. Ideally, the coefficients would be found from empirical testing of sCO_2 turbomachines and correlated against dimensionless parameters such as specific speed or flow coefficient. However, such empirical data does not exist yet for sCO_2 turbomachinery. It is also conceivable that CFD simulations could be performed in lieu of experiments to find appropriate correlations. Indeed, any method that provides values for the three loss coefficients and the slip factor can be used to complete the models.

To demonstrate this, the commercial turbomachinery package CompAero [16] was used to find values for the loss coefficients and the slip factor. CompAero is a widely recognised compressor design tool and is based on the work of Aungier [3].

The software is clearly intended to work with gases and gas mixtures as working fluid and therefore its accuracy in predicting sCO_2 turbomachinery performance is untested.

However, even without support for sCO_2 CompAero is still a useful tool because it provides detailed information about the geometry and performance of the compressor and the thermodynamic properties are evaluated at all flow stations.

The following method was applied to find the values of the loss coefficients and the slip factor.

1. An arbitrary compressor was designed in CompAero, using CompAero's default values and the typical values suggested by Aungier [3]. Vapour CO_2 was used as the working fluid. The specifications of this compressor are given in the first part of Table 1 under the heading *Design specifications*.
2. The thermodynamic properties at the tip of the rotor and at the outlet of the stage, as well as the fluid work are recorded. These values are presented in the second part of Table 1 under the heading *Measurements used for calibration*.
3. In the compressor model of this work, the design specifications and the performance metrics are entered and treated as constant values whereas all the other variables including the loss coefficients and the slip factor are treated as free variables. The thermodynamic property correlations for sCO_2 in the model are replaced with thermodynamic properties for CO_2 in the vapour phase.
4. The model is solved numerically by running the optimisation algorithm for an arbitrary objective function. If a sufficient number of starting points are given, the optimisation algorithm finds a unique solution (within the constraint tolerance) for the compressor. The values for the loss coefficients and the slip factor can then be found from the models. In this way, the compressor model of this work is calibrated with the compressor model of CompAero. For the arbitrary design that was used for the calibration, the values for the loss coefficients and the slip factor are presented in the third part of Table 1 under the heading *Coefficients*.

Given the geometry of a turbomachine, its inlet conditions and two additional independent variables, then the operating condition of a turbomachine can be uniquely determined [7]. Once values for the loss coefficients and the slip factor are given as constant values to the model, then this condition becomes true for the models in this work.

Therefore, if only the values of the first and third part of Table 1 are supplied to the model, then the values of the second part as well as all the other thermodynamic properties, velocity components and flow angles can be uniquely determined.

DOI: 10.17185/duepublico/48895

Moreover, the model will give the same numerical values as the second part of Table 1, representing an error of zero with the CompAero design that has been used to calibrate the model. Since it is possible to achieve zero error only by adjusting the values for the loss coefficients and the slip factor, the models of this work can be considered as verified.

Table 1: design variables of an arbitrary compressor used for calibration of the model loss coefficients and slip factor

Design specifications	**Value**
Tip radius, r_2	74.5 mm
Hub radius, r_{3h}	26.1 mm
Shroud radius, r_{3s}	62.5 mm
Blade width, b_2	9.53 mm
Diffuser exit area, A_1	6 880 mm^2
Inlet total temperature, T_{03}	300 K
Inlet total pressure, P_{03}	130 kPa
Absolute flow angle at rotor inlet, α_3	0.00°
Physical blade angle at tip, β_2'	-35.1 °
Mass flow rate, $\dot{m}$	2.80 kg/s
Angular velocity, ω	55 000 rpm
Measurements used for calibration	**Value**
Tip total temperature, T_{02}	410 K
Tip total pressure, P_{02}	406 kPa
Stage exit total temperature, T_{01}	410 K
Stage exit total pressure, P_{01}	341 kPa
Fluid power, $\dot{W}_F$	275 kW
Coefficients	**Value**
Rotor loss coefficient, ζ_R	0.619
Parasitic work coefficient, ζ_P	0.0108
Diffuser efficiency, η_D	0.972
Slip factor, σ	0.808

Table 2: design variables and observed errors for an arbitrary compressor, using loss coefficients and slip factor calibrated to a different compressor

Design specifications		**Value**	
Tip radius, r_2		41.3 mm	
Hub radius, r_{3h}		14.5 mm	
Shroud radius, r_{3s}		27.0 mm	
Blade width, b_2		3.88 mm	
Diffuser exit area, A_1		1 580 mm^2	
Inlet total temperature, T_{03}		300 K	
Inlet total pressure, P_{03}		130 kPa	
Absolute flow angle at rotor inlet, α_3		0.00°	
Physical blade angle at tip, β_2'		-40.3°	
Mass flow rate, $\dot{m}$		0.36 kg/s	
Angular velocity, ω		80 000 rpm	
Results	**CompAero**	**This work**	**Error**
Tip total temperature, T_{02}	388 K	385 K	0.8%
Tip total pressure, P_{02}	375 kPa	370 kPa	1.3%
Stage exit total temperature, T_{01}	388 K	384 K	1.0%
Stage exit total pressure, P_{01}	284 kPa	321 kPa	13%
Fluid power, $\dot{W}_F$	28.0 kW	26.3 kW	6.1%

Although the values for the loss coefficients and slip factor presented in Table 1 produce zero error for that particular compressor design, it is to be expected that if a different compressor design is used with the same coefficient values then some error in the results will be observed.

In the first part of Table 2, the design specifications of another arbitrary compressor are given. The specifications have been entered as constant values in the compressor model of this work, together with the values of the loss coefficients and slip factor presented in the third part of Table 1. The model was solved numerically by running the optimisation algorithm for an arbitrary objective function. Again, several starting points are needed but the algorithm is able to find a unique solution for this compressor.

The results of the thermodynamic properties at the tip and at the stage outlet, and the fluid work from the model are compared with the values that CompAero has calculated they should be. Errors for the different results of between 0.8% and 13% are observed, with the greatest error observed for the stage outlet pressure.

Given an arbitrary compressor, the model can be calibrated to produce zero error. However, if the same calibrated model is applied to a different arbitrary compressor, some error is introduced. This confirms that a constant value for each loss coefficient and the slip factor cannot possibly be accurate for all compressor designs. It is necessary to replace the constant values with correlations against non-dimensional parameters developed from the results of CFD simulations or empirical tests of a wide variety of compressor designs. This is beyond the scope of the current work, but it should be clear that once such correlations are developed then they can easily be implemented in the models that have been presented.

Notice that the performance metrics used to calibrate the models are very general: total temperature and total pressure measurements are easy to measure on an experimental test bench and so is shaft power (CompAero only provides fluid power $\dot{W}_F$ and not the required shaft power $\dot{W}$ although in an experimental test the fluid power would not be known but the shaft power can easily be measured).

Therefore, regardless of whether experiments or CFD simulations are performed, the calibration method proposed in this work can be used to develop more generalised correlations for the loss coefficients and slip factor.

RESULTS

Two case studies will be presented which demonstrate the optimisation of a centrifugal compressor and a radial inflow turbine. In Table 3 the specifications of a typical sCO_2 compressor design case are presented.

Table 3: specifications of a typical compressor design case

Design specifications	**Value**
Stage inlet total temperature, T_{03}	335 K
Stage inlet total pressure, P_{03}	8.50 MPa
Absolute flow angle at rotor inlet, α_3	0.00°
Total-to-total pressure ratio, PR_0	2.50

DOI: 10.17185/duepublico/48895

The inlet temperature and pressure to the stage are close to (but not at) the critical conditions for CO_2, the flow enters the rotor section without incidence, and the required total-to-total pressure ratio is provided. The compressor designer is now tasked with finding the geometry of a compressor capable of achieving this pressure ratio at the stated conditions.

To assess the quality of candidate compressor designs, an objective function is required. A typical objective function might be to

- minimise the required shaft power $\dot{W}$,
- minimise the required angular velocity ω,
- maximise the mass flow rate $\dot{m}$ throughput, or
- minimise the tip radius r_2.

It is however unlikely that any of these objectives would be prioritised without consideration for the others, which therefore makes this a multi-objective optimisation problem. Multi-objective optimisation problems typically do not have a single global optimal solution and instead a range of optimal solutions exist which lie on the so-called *Pareto front*. Any point on the Pareto front is referred to as a *Pareto-optimal* point. Pareto-optimal points represent a solution which is optimal for at least one of the variables in the objective function.

Consider the results of the compressor optimisation on a plot of angular velocity against shaft power in Figure 4. Every point on the plot represents a valid solution or design that the designer is able to select – a *local minimum* of the optimisation problem. Most designs however are inferior and only the designs on the Pareto front should be considered. Every point on the Pareto front in Figure 4 represents a design which either minimises the shaft power at a particular angular velocity or minimises the angular velocity at a particular shaft power.

The general trend that the Pareto front shows is that as shaft power is reduced, angular velocity must increase in order to sustain the required pressure ratio.

The large spread that is visible in the data shows that in general shaft power and angular velocity are poorly correlated for a compressor at a constant pressure ratio. The geometry of the compressor has a significant effect on the relationship between these two variables.

In comparison, the mass flow rate plotted against shaft power in Figure 5 shows a much smaller spread in the data, especially at lower power ratings. The conclusion of this is that mass flow rate is a much more dominant variable than angular velocity for a compressor at a constant pressure ratio. The Pareto-front in Figure 5 shows that there is a linear relationship between mass flow rate and shaft power as is to be expected: as the required mass flow rate increases the shaft power must increase proportionally. It is interesting to note however that at higher power ratings the influence of the compressor's geometry plays a very significant role in determining the mass flow rate that can be achieved. If the Pareto-optimal design at a power rating of 10 MW is selected, then the mass flow rate can be as high as 220 kg/s; but if a poor design is selected then the mass flow rate can be up to 100 kg/s lower. At smaller power ratings, the influence of geometry is not as important in absolute terms, but since the achievable mass flow rates are lower the influence of geometry remains considerable.

The location of the Pareto-optimal point of Figure 4 on Figure 5 is indicated by the dotted-lines, which show the point to be close to or on the Pareto front in Figure 5 as well. The Pareto front in Figure 5 represents all designs which either maximise the mass flow rate at a given shaft power or minimise the shaft power at a given mass flow rate.

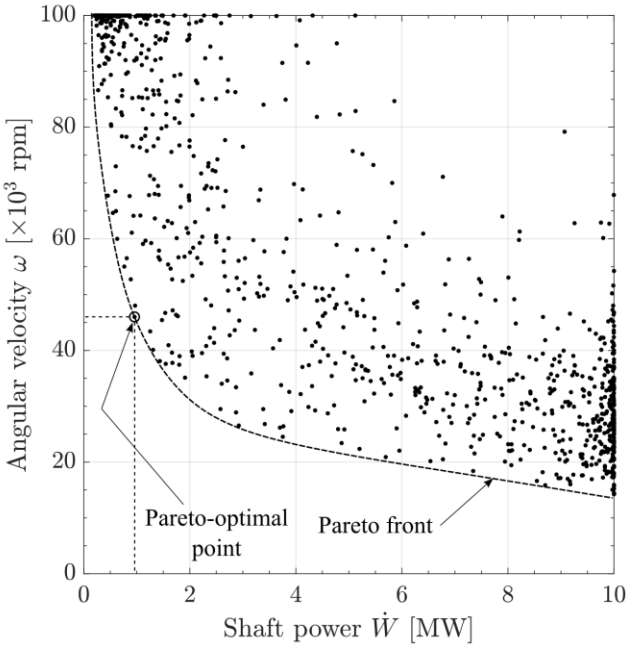

Figure 4: compressor angular velocity vs shaft power

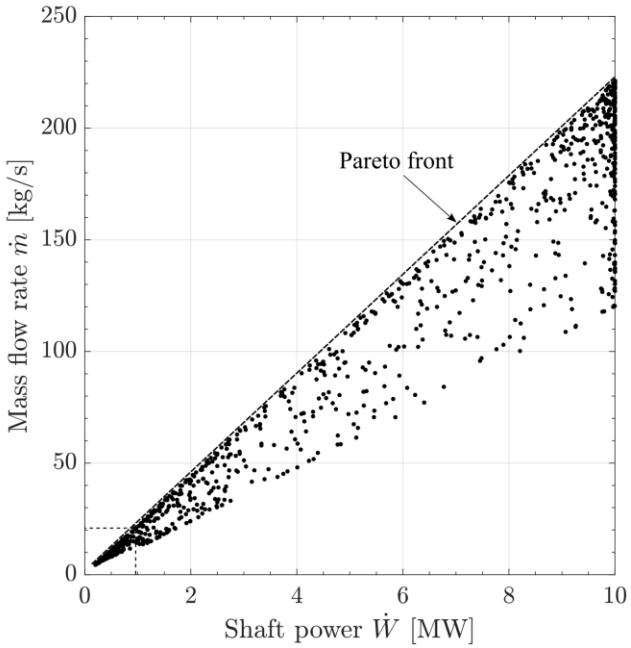

Figure 5: compressor mass flow rate vs shaft power

DOI: 10.17185/duepublico/48895

An even better correlation in the data can be seen if tip radius is plotted against angular velocity, as in Figure 6. The data shows a very narrow spread and the overall trend is very clear: in order to maintain a constant pressure ratio, as the compressor speed is reduced the tip radius has to increase. This relationship is only marginally affected by the other variables of the compressor's design.

However, even though the overall trend is clear, consider that if a tip radius of 30 mm is selected, the angular velocity can still be anywhere in the range of about 70 000 rpm to 100 000 rpm (and potentially even higher since 100 000 rpm was the upper bound on angular velocity for the optimisation) which is a very significant difference in practice. This highlights the importance of optimisation, as using a poor design could result in the compressor having to operate much faster than it needed to in order to achieve the required pressure ratio.

The Pareto front in Figure 6 shows the designs which either minimise tip radius at a given angular velocity or minimise angular velocity at a given tip radius.

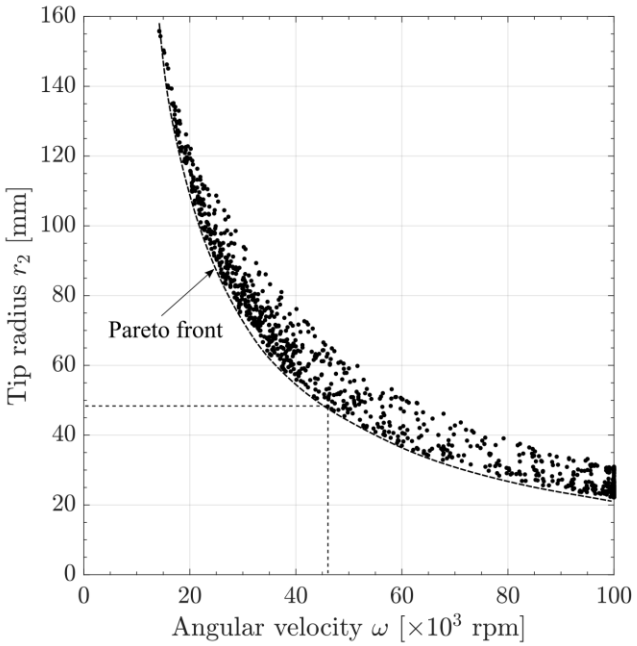

Figure 6: compressor tip radius vs angular velocity

The Pareto-optimal point of Figure 4 is shown in Figure 6 by the dotted lines and once again it lies on the Pareto front in Figure 6 as well. It is not a general rule that in a multi-objective optimisation problem that a point on one Pareto front would also lie on other Pareto fronts, but in this case it would appear as if a compressor design which is Pareto-optimal on the angular velocity vs shaft power plot is also Pareto-optimal on the mass flow rate vs shaft power plot and on the tip radius vs angular velocity plot.

In Table 4 selected results for the Pareto-optimal compressor design (identified in Figure 3) are provided.

Table 4: selected results of an optimised compressor design

Design results	Value
Tip radius, r_2	48.3 mm
Hub radius, r_{3h}	12.2 mm
Shroud radius, r_{3s}	32.0 mm
Blade width, b_2	4.83 mm
Mass flow rate, $\dot{m}$	21.2 kg/s
Angular velocity, ω	46 000 rpm
Shaft power, $\dot{W}$	958 kW

The second case study to be considered in this work concerns the design of a radial inflow turbine. In Table 5 the specifications of a typical sCO_2 turbine design case are given, including the stage inlet temperature and pressure. Additionally, the design is required to have no absolute tangential velocity component at the outlet of the rotor; and the rotor tip radius is required to be a specific value (an example of where this might be relevant specification is when a new rotor has to be designed to work with a previously designed volute/scroll section).

Table 5: specifications of a typical turbine design case

Design specifications	Value
Stage inlet total temperature, T_{01}	850 K
Stage inlet total pressure, P_{01}	25.0 MPa
Absolute flow angle at rotor outlet, α_3	0.00°
Rotor tip radius, r_2	75.0 mm

The task of the turbine designer is to find the geometry of a turbine that meets these specifications but also that

- maximises the generated shaft power $\dot{W}$,
- minimises the angular velocity ω,
- minimises the required mass flow rate $\dot{m}$, and/or
- maximises the total-to-static isentropic efficiency $\eta_{s,ts}$ (which is the ratio of the actual power produced to the power that would have been produced if the turbine was isentropic and if its diffuser reduced the flow velocity to zero)

Figure 7 shows the optimisation results of this case study, with angular velocity plotted against mass flow rate. Despite also being a multi-objective optimisation problem, in this case angular velocity and mass flow rate can both be minimised simultaneously – at zero flow. Clearly, this is an unpractical choice even though it is a valid solution based on the constraints of the problem and the specifications that were provided. As the flow and speed increase, the spread in the data also increases and two diverging fronts are created. On front 1 are the turbine designs which minimise angular velocity for a given mass flow rate and on front 2 are the turbine designs which minimise mass flow rate for a given angular velocity. These are *fronts* rather than *Pareto fronts* because on a Pareto front no global optimum exists and all solutions can be treated equally. In this case, a global optimum (for the relationship between angular velocity and mass flow rate) does exist but it lies at a point that does not represent a practical design; and a design that is selected on one of the fronts will be optimal for one metric but not for the other.

DOI: 10.17185/duepublico/48895

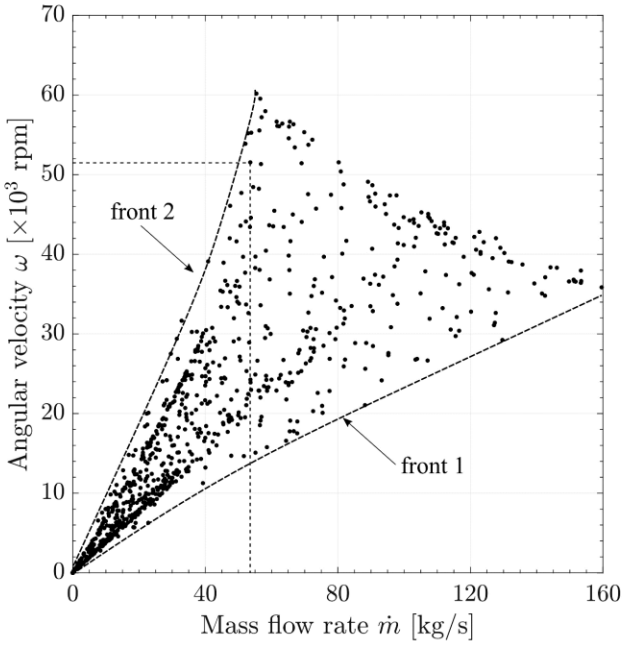

Figure 7: turbine angular velocity vs mass flow rate

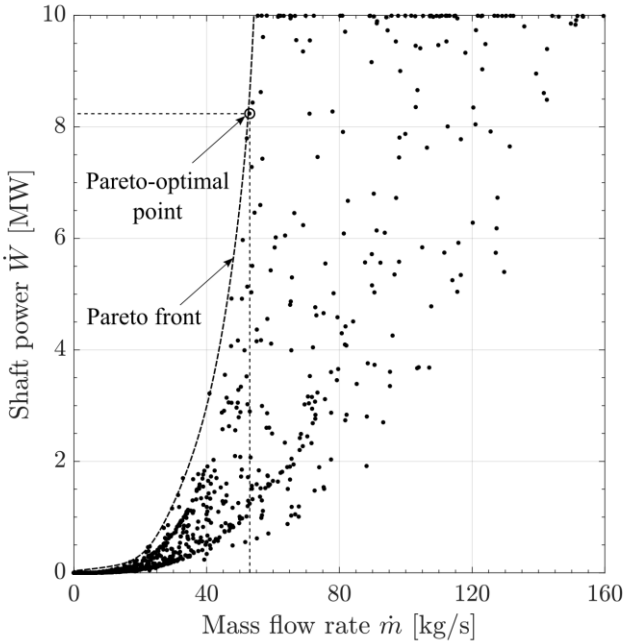

Figure 8: turbine shaft power vs mass flow rate

A Pareto front can however be identified if power output is plotted against mass flow rate, as in Figure 8. The Pareto front corresponds to turbine designs in which the power output at a given flow rate is maximised or in which the mass flow rate for a given power output is minimised. The Pareto front is practically zero for low mass flow rates but rises sharply from about 20 kg/s. The front becomes almost vertical by the time it reaches a power output of 10 MW (the upper bound that was considered in this case) at a mass flow rate of 55 kg/s, indicating that beyond this point the Pareto-optimal power output is no longer dominated by the mass flow rate.

However, the large spread in the data is indicative that the other design variables of the turbine have a significant effect on the mass flow rate that is required to produce a particular power output. At 10 MW, the Pareto-optimal design requires 55 kg/s of mass flow through it, but a poor design can require a mass flow rate that is three times as much.

A Pareto-optimal turbine design is selected in Figure 8 and indicated by the dotted lines. This same design is also indicated by the dotted lines in Figures 7 and 9.

In Figure 9, the total-to-static isentropic efficiency of the turbine designs are presented. It can be seen that the efficiencies are very high and even the poor designs have efficiencies that exceed 85%. There are three reasons for this; the first is that the design limits for angles, velocity ratios and geometry ratios [8] proved to be effective for eliminating the worst designs. Secondly, constant loss coefficients were used which means – based on the definitions in Equations 12 and 13 – that simply by reducing the relative velocity at the tip the losses can be minimised. More accurate loss coefficients that are actually correlated against geometrical and flow parameters will ensure that the losses cannot be minimised by minimising a single term.

The third reason is that the allowable diffuser outlet area was very large (up to 1.6 m^2 was allowed, compared to blade dimensions which were restricted to a maximum of 0.5 m). As the area ratio of a diffuser increases, in general its ability to recover kinetic energy also increases. Therefore, the designs with high efficiencies typically have large diffusers as well.

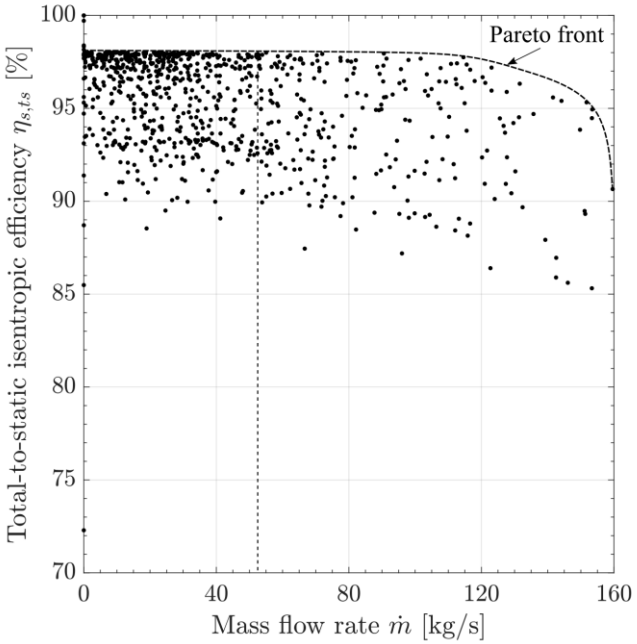

Figure 9: turbine efficiency vs mass flow rate

DOI: 10.17185/duepublico/48895

The Pareto front in Figure 9 (which indicates the designs that maximise efficiency for a given mass flow rate) is practically horizontal up to 120 kg/s. This shows that the highest efficiency can be achieved regardless of mass flow rate. However, the front drops at higher mass flow rates and this can be attributed to certain variables reaching their upper or lower bounds. For example, for some turbines at these high mass flow rates the diffuser exit area that is required for a high efficiency is larger than the given upper bound of 1.6 m^2.

In Table 6 selected results for the Pareto-optimal turbine design (identified in Figure 8) are provided.

Table 6: selected results of an optimised turbine design

Design results	**Value**
Hub radius, r_{3h}	16.1 mm
Shroud radius, r_{3s}	40.2 mm
Blade width, b_2	7.64 mm
Mass flow rate, $\dot{m}$	52.9 kg/s
Total-to-total pressure ratio, PR_0	1.83
Angular velocity, ω	55 000 rpm
Shaft power, $\dot{W}$	8.24 MW

APPLICATION

Once the general relationships between the major design variables of the turbomachines have been studied from the results above, it is up to the designer to select one of the designs or to change the given specifications or constraints and re-run the optimisation algorithm if the results are not satisfactory.

In this work, every compressor design is made up of 97 design variables; and every turbine design is made up of 111 design variables (the turbine requires more variables because section 4-3 is ignored for the compressor). The values of all these design variables for all the valid designs are stored on file. Once a candidate design is identified, then the designer can find the values for its other design variables from the file.

The choice of the design variables to specify and to plot on the graphs in this work is arbitrary and purely for the sake of demonstration. It is in fact possible to specify any combination of variables or to plot the results of any combination of design variables against each other. Once all of the equations of the models are expressed and the thermodynamic property correlations are added, the compressor model consists of 82 equality and 9 inequality constraints, and the turbine consists of 92 equality and 10 inequality constraints. These constraints and the choices of the upper and lower bounds on the variables influence which feasible designs are possible and what the design space that is available to the designer looks like. Therefore, choosing an optimal compressor or turbine design begins with properly defining the objective function(s) and choosing practical and realistic upper and lower bounds on the variables (a variable that is specified as a constant value has an equal upper and lower bound).

Ideally, the design space should be restricted as much as possible before running the optimisation algorithm.

In the turbine case study example, only a tip radius was specified but the required power rating, angular velocity or mass flow rate was not given. This led to the optimisation algorithm proposing unrealistically low mass flow rates as valid solutions. Whilst these are valid solutions indeed, it shows that optimisation is only useful insofar as the exact problem to be solved can be accurately identified.

CONCLUSION

Models for a centrifugal compressor and a radial inflow turbine have been developed based on the classical mean-line velocity triangle approach. The models can be used as an alternative to the proven CFD/RSM optimisation methods.

Restrictive assumptions were not made and correlations of fluid thermodynamic properties were generated from tabulated data. The loss coefficients and slip factor were calibrated against a compressor design from the commercial compressor design software CompAero. No difference was observed between the current compressor model and the CompAero model if the loss coefficients and slip factor were calibrated, but errors of up to 13% were observed if the same loss coefficients and slip factor were used to model another arbitrary compressor design.

Two typical design optimisation case studies were presented: one for a centrifugal compressor that was required to develop a fixed pressure ratio and one for a radial inflow turbine that was required to have a fixed tip radius. The results of the compressor case study showed that Pareto-optimal solutions could be identified on the angular velocity vs shaft power plot, the mass flow rate vs shaft power plot and the tip radius vs angular velocity plot. The results of the turbine case showed for a constant radius turbine minimising angular velocity and minimising mass flow rate are diverging objectives and Pareto-optimal solutions do not exist; although a global optimum exists at zero mass flow rate. Pareto-optimal solutions could be identified on the shaft power vs mass flow rate plot however, as well as on the efficiency vs mass flow rate plot. The high efficiencies in the latter plot highlighted the inaccuracies with using constant loss coefficients instead of correlations.

The models in this work can be applied equally well to other working fluids and the rather general results of this work are surely not applicable to sCO_2 only. The proposed methodology is however especially useful for sCO_2 turbomachinery optimisation because the industry is still in its infancy.

FUTURE WORK

Extensive CFD simulations or experiments on a wide variety of sCO_2 turbomachinery designs should be performed from which accurate and widely applicable correlations for the loss coefficients against non-dimensional flow parameters could be developed. These correlations could be developed using the methodology proposed in this work, and the constant coefficients applied as an example in this work should be supplemented with the developed correlations. Once such correlations have been developed, the presented models can be used additionally for off-design performance modelling, without the need for any changes to be made to the underlying computational implementation.

DOI: 10.17185/duepublico/48895

NOMENCLATURE

Letters

A	area (m^2)
AR	area ratio (-)
B	blade velocity (m/s)
b	blade width (m)
C_p	pressure recovery coefficient (-)
f	objective function
g	inequality constraint
h	enthalpy (J/kg); equality constraint
M	moment (Nm)
m	meridional direction
$\dot{m}$	mass flow rate (kg/s)
P	pressure (Pa)
PR	pressure ratio (-)
R	relative velocity (m/s)
r	radius (m); radial direction
T	temperature (K)
t	tolerance (-); tangential direction
V	velocity (m/s)
$\dot{W}$	power (W)
w	energy/work (J)
x	variable; axial direction
$\check{x}$	lower bound on variable
$\hat{x}$	upper bound on variable
x_0	starting point

Symbols

α	absolute flow angle (degrees)
β	relative flow angle (degrees)
ζ	loss coefficient (-)
η	efficiency (-)
θ	generic angle (degrees)
ρ	density (kg/m^3)
σ	slip factor (-)
ω	angular velocity (rad/s)

Subscripts

C	compressor
c	constraint
D	diffuser
F	fluid
h	hub
m	meridional direction
P	parasitic
R	rotor
r	radial direction
s	shroud, isentropic
T	turbine
t	tangential direction
ts	total-to-static
x	axial direction
0	total state
1	station 1
2	station 2 (tip)
3	station 3 (eye)
4	station 4

ACKNOWLEDGEMENTS

This work has been financially supported by the Solar Thermal Energy Research Group (STERG) based at Stellenbosch University.

REFERENCES

[1] V. Dostal, M. J. Driscoll, and P. Hejzlar, "A Supercritical Carbon Dioxide Cycle for Next Generation Nuclear Reactors," *Technical Report MIT-ANP-TR-100*, 2004.

[2] M. J. Hexemer and K. Rahner, "Supercritical CO2 Brayton Cycle Integrated System Test (IST) TRACE Model and Control System Design," in *Supercritical CO2 Power Cycle Symposium*, 2011.

[3] R. H. Aungier, *Centrifugal Compressors: A Strategy for Aerodynamic Design and Analysis*. New York, NY: ASME Press, 2000.

[4] Z. Li and X. Zheng, "Review of design optimization methods for turbomachinery aerodynamics," *Progress in Aerospace Sciences*, vol. 93, pp. 1–23, 2017.

[5] M. C. Duta and M. D. Duta, "Multi-objective turbomachinery optimization using a gradient-enhanced multi-layer perceptron," *International Journal for Numerical Methods in Fluids*, vol. 61, pp. 591–605, 2009.

[6] X. D. Wang, C. Hirsch, S. Kang, and C. Lacor, "Multi-objective optimization of turbomachinery using improved NSGA-II and approximation model," *Computer Methods in Applied Mechanics and Engineering*, vol. 200, pp. 883–895, 2011.

[7] S. L. Dixon and C. A. Hall, *Fluid Mechanics and Thermodynamics of Turbomachinery*, 7th ed. Oxford, United Kingdom: Butterworth-Heinemann, 2014.

[8] S. A. Korpela, *Principles of Turbomachinery*. Hoboken, NJ: Wiley, 2011.

[9] D. Japikse and N. C. Baines, *Introduction to Turbomachinery*. Norwich, VT: Concepts ETI, Inc., 1994.

[10] F. M. White, *Fluid Mechanics*, 7th ed. New York, NY: McGraw-Hill, 2011.

[11] R. Persky and E. Sauret, "Loss models for on and off-design performance of radial inflow turbomachinery," *Applied Thermal Engineering*, vol. 150, pp. 1066–1077, 2019.

[12] L. Da Lio, G. Manente, and A. Lazzaretto, "A mean-line model to predict the design efficiency of radial inflow turbines in organic Rankine cycle (ORC) systems," *Applied Energy*, vol. 205, pp. 187–209, 2017.

[13] F. Alshammari, A. Karvountzis-Kontakiotis, A. Pesiridis, and P. Giannakakis, "Off-design performance prediction of radial turbines operating with ideal and real working fluids," *Energy Conversion and Management*, vol. 171, pp. 1430–1439, 2018.

[14] J. A. Snyman, *Practical Mathematical Optimization*. Pretoria, South Africa: University of Pretoria, 2004.

[15] The Mathworks Inc., "Matlab R2018b Documentation." 2018.

[16] R. H. Aungier, "CompAero 2.00." Flexware, Grapeville, PA, 2011.

DOI: 10.17185/duepublico/48895

DOI: 10.17185/duepublico/48895
URN: urn:nbn:de:hbz:464-20191004-103834-4